Neurocomputing 73 (2010) 927–936

Contents lists available at ScienceDirect

Neurocomputing

journal homepage: www.elsevier.com/locate/neucom

Object-oriented subspace analysis for airborne hyperspectral remote sensing imagery

Liangpei Zhang, Xin Huang *

The State Key Laboratory of Information Engineering in Surveying, Mapping and Remote Sensing, Wuhan University, PR China

ARTICLE INFO

Article history:
Received 7 May 2009
Received in revised form
3 September 2009
Accepted 8 September 2009
Communicated by X. Li
Available online 17 October 2009

Keywords:
Hyperspectral images
Subspace analysis
Feature extraction
Object-oriented analysis
Texture

ABSTRACT

An object-oriented mapping approach based on subspace analysis of airborne hyperspectral images was investigated in this paper. Hyperspectral features were extracted based on subspace learning approaches, in order to reduce the redundancy of spectral space and extract the characteristic images for the further object-oriented classification. In this paper, three kinds of spectral feature extraction (FE) methods were utilized to obtain the subspace of airborne hyperspectral data: (1) unsupervised FE, such as PCA (principal component analysis), ICA (independent component analysis) and MNF (maximum noise fraction); (2) supervised FE, e.g. DBFE (decision boundary feature extraction), DAFE (discriminant analysis feature extraction) and NWFE (nonparametric weighted feature extraction); and (3) linear mixture analysis. Afterwards, the extracted subspace features were fed into the object-based classification system. The FNEA (fractal net evolution approach) was utilized to extract objects from the subspace images and SVM (support vector machines) was then used to classify the object-based features. Experiments were conducted on two airborne hyperspectral datasets: (1) the AVIRIS dataset over the northwest Indiana's Pine with 220 spectral bands (agricultural region), and (2) the ROSIS dataset over Pavia University, northern of Italy with 102 spectral bands (urban region). Results revealed that the proposed object-based approach could give significantly higher accuracies than the traditional pixel-based subspace classification.

1. Introduction

Hyperspectral sensors record the spectrum of solar radiation reflected by the Earth's surface. The value of using a hyperspectral sensor lies in its ability to provide a high-resolution reflectance spectrum for each pixel in the image [1]. The hyperspectral data provide contiguous or noncontiguous 10 nm bands throughout the 400–2500 nm region of the electromagnetic spectrum, and hence it is potential to precisely discriminate different land cover types using the sufficient spectral information. Such identification is of great significance for detecting minerals, precision farming, and urban planning, etc.

However, the high-dimensional feature space of hyperspectral data poses challenges to image processing and classification techniques. The problem is due to the high number of spectral channels and the relatively small number of labels samples. Therefore, feature extraction (FE) methods are commonly used to reduce the data dimensionality and computational cost. Many algorithms have been reported to be effective in reducing the dimensions of input space and achieving better performance, such as linear and nonlinear principal component analysis (PCA) [2,3], linear discriminant analysis (LDA) [4,5], locally linear embedding (LLE) [6], non-negative matrix factorization (NMF) [7], wavelet feature extraction [8], and independent component analysis (ICA) [9]. More recently, Tao et al. [10] proposed a tensor rank one discriminant analysis (TR1DA) for feature selection and pattern classification, which allows more effective image representation with a relatively small number of parameters. Tao et al. [11] pointed out that although the Fisher's LDA was one of the important subspace methods, for the c-class problem, it had a tendency to merge nearby classes under projection of the feature space since the dimension of the projected subspace was lower than c-1. Consequently, they proposed three new criteria for subspace selection based on the geometric mean of the divergences between different classes. Li et al. [12] proposed a new manifold learning technique called discriminant locally linear embedding (DLLE), in order to preserve the local geometric properties within each class and enhance the separability between different classes. Furthermore, the miltilinear version of DLLE was also proposed for the out-of-sample problem with high-order tensor input.

By summarizing the exiting literature about subspace extraction and classification methods, it can be found that it always focuses on the pixel-based classification, without considering the

* Corresponding author.
E-mail address: huang_whu@163.com (X. Huang).

0925-2312/$ - see front matter © 2009 Elsevier B.V. All rights reserved.
doi:10.1016/j.neucom.2009.09.011

spatial relationship of neighboring pixels. The pixel-based approach often results in pepper–salt effects [7] and it is difficult to discriminate the spectrally similar objects when contextual information is not considered. Recent studies show that the exploitation of spatial information is necessary for classification of hyperspectral imagery, but few such approaches have been proposed [13], which is partly due to the high dimensionality of the data and the spectral and spatial heterogeneity of remote sensing images [14]. In this context, the objective of this research is to exploit both spectral and spatial information contained in the hyperspectral remote sensing images, in order to precisely map land covers. To this end, we propose an object-oriented subspace analysis approach for classification of airborne hyperspectral remote sensing data. The flow chart is shown in Fig. 1. The proposed framework consists of two blocks:

(1) Subspace extraction for pre-processing: it aims to reduce the dimensionality and extract the spectral subspace from hyperspectral data. In this paper, three kinds approaches are employed, including unsupervised and supervised FE, and the linear spectral unmixing (LSU).
(2) Object-based analysis (OBA) of the spectral subspace: the object-oriented approach is used to classify the subspace features, and take the spatial and contextual information into account for classification. The basic idea of OBA is to group the spatially adjacent pixels into spectrally homogeneous objects and then conduct classification on objects as the minimum processing unit. In this paper, the fractal net evolution approach (FNEA) [15] was utilized to extract objects from subspace images and SVM was then used to classify the object-based subspace features. SVM is of interest due to its insensitivity to the high dimensionality of the feature space and the adaptive and fast learning ability [16,17].

The experiments were conducted on two airborne hyperspectral datasets: (1) the AVIRIS (Airborne Visible/Infrared Imaging Spectrometer) hyperspectral dataset over the Indian Pines test site (agricultural region) and (2) the ROSIS (Reflective Optics System Imaging Spectrometer) hyperspectral image over Pavia University, northern of Italy (urban region). In experiments, the classification accuracies resulted from the pixel-based and object-based subspace were compared and analyzed. In addition, GLCM (gray level co-occurrence matrix), and wavelet-based texture features were implemented based on the extracted subspace images, and the results were used as benchmarks to evaluate the proposed algorithm.

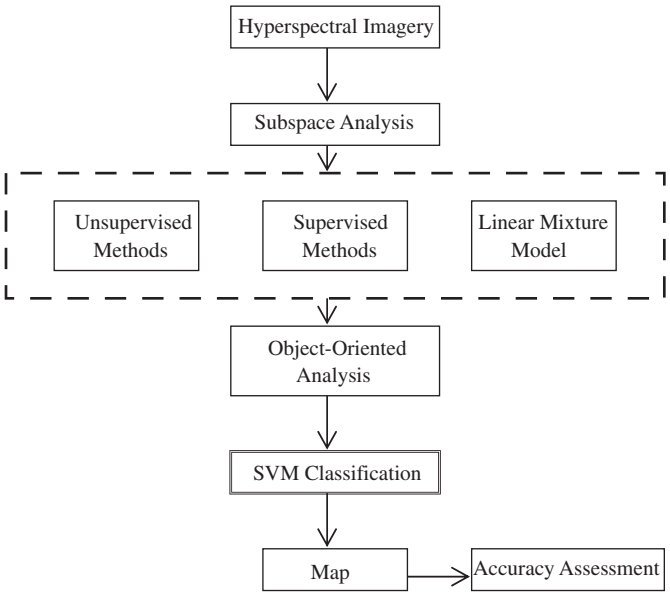

Fig. 1. Flow chart for the object-oriented classification approach of the spectral subspace of hyperspectral remote sensing images.

The remainder of this paper was organized as follows. Section 2 introduced the unsupervised/supervised subspace analysis methods and the linear spectral unmixing. The proposed object-oriented subspace analysis and classification framework was described in Section 3. Section 4 presented the experimental results and comparisons, and the last section concluded.

2. Subspace feature extraction

2.1. Unsupervised FE

(1) PCA (principal component analysis)

The PC images of a hyperspectral data can be calculated as:

$$z_{pca} = V^T(z - m) \tag{1}$$

where m is the mean, and z and z_{pca} are pixel vectors before and after the PCA transformation, respectively. $V = [v_1, v_2, \ldots, v_B]$ is the eigenvector of the hyperspectral data covariance matrix Σ, and it can be expressed as:

$$V^T \Sigma V = \Lambda \tag{2}$$

where $\Lambda = [\lambda_1, \lambda_2, \ldots, \lambda_B]$ is the eigenvalue matrix of Σ, and B is the number of hyperspectral channels. PCA has been shown not to be optimal for classification and it is also not appropriate for material identification and separability. However, from the feature extraction point of view, PCA can represent the hyperspectral feature space using several principal components. In addition, it is interesting to test the performance of PCA when the neighboring pixels are considered for classification.

(2) ICA (independent component analysis)

Recently, ICA-based blind source separation technique has received attention for hyperspectral remote sensing imagery. The goal of ICA is to recover independent sources given only sensor observations that are unknown linear mixtures of the unobserved independent source signals [18]. In contrast to correlation-based transformations such as principal component analysis (PCA), ICA not only decorrelates the signals (2-order statistics) but also reduces higher-order statistical dependences, attempting to make the signals as independent as possible [18].

The basic model of ICA is:

$$x = A \cdot s \tag{3}$$

where $x = [x_1, \ldots, x_n]^T$ is an observation vector, A is an $n \times m$ mixing matrix, and $s = [s_1, \ldots, s_m]^T$ are mutually independent components. ICA aims to find a linear transformation matrix W such that the sources can be estimated from the observed vector x by optimizing the statistical independence criterion,

$$u = W \cdot x \tag{4}$$

where u is an estimate of the sources. Starting from an information theoretic viewpoint, the ICA problem is formulated as the minimization of mutual information between the transformed variables, since mutual information is a natural measure of the dependence between random variables. ICA is a frequently used unsupervised feature extraction method, and it shows good classification ability, however, it is difficult to determine the appropriate dimensionality of ICs. Quite a few ICA algorithms exist. In this study, the information maximization [19] is used to

extract the spectral subspace from the airborne hyperspectral images.

(3) MNF (maximum noise fraction)

PCA chooses the new components by maximizing variance, which is questionable since the variance can be contributed from both signals and noise. MNF is an improved version of PCA, and it is a subspace extraction technique in terms of image quality (signal-to-noise ratio) [20]. It is able to determine the inherent dimensionality of feature space, to segregate noise in the data, and to reduce the computational cost for subsequent processing. MNF is based on the additive noise model:

$$Z(x) = S(x) + N(x) \tag{5}$$

where $Z(x)$ is the original signal, and $S(x)$ and $N(x)$ are the uncorrelated signal and noise components of $Z(x)$, respectively. The covariance matrices can be related by:

$$\mathrm{Cov}(Z(x)) = \Sigma = \Sigma_S + \Sigma_N \tag{6}$$

where Σ_S and Σ_N are the signal and noise covariance matrices, respectively. The noise fraction for band b is defined as: $\mathrm{Var}(N_b(x))/\mathrm{Var}(Z_b(x))$. MNF transformation results in new uncorrelated images based on a linear transformation of the original data set: $Y = A^T Z$ where the transformation matrix A is calculated by solving the eigenvalue equation:

$$A\Sigma_N\Sigma^{-1} = \Lambda A \tag{7}$$

where $\Lambda = (\lambda_1, \lambda_2, \ldots, \lambda_B)$ is a diagonal matrix of the eigenvalues. The MNF transformation arranges the feature bands with decreasing noise fraction, therefore, the subspace of a hyperspectral image can be extracted by analyzing the proportion of the noise variance described by the first several MNF bands. Consequently, the hyperspectral feature space can be divided into two parts: one part associated with large eigenvalues and coherent eigenimages, and a complementary part with near-unity eigenvalues and noise-dominated images. By using only the coherent portions, the noise is separated from the data, thus improving performance of spectral analysis.

2.2. Supervised FE

(1) DAFE (discriminant analysis feature extraction)

DAFE is a well-known feature extraction method to enhance separability of the subspace [21]. It is based on the maximization of separability by defining a within-class matrix Σ_W and a between-class scatter matrix Σ_B:

$$J = \mathrm{tr}(\Sigma_W^{-1}\Sigma_B) \tag{8}$$

where $\mathrm{tr}(\cdot)$ is the trace of a matrix. The transformation matrix can be expressed by the normalized eigenvectors of $\Sigma_W^{-1}\Sigma_B$ corresponding to the eigenvalues in a decreasing order.

(2) DBFE (decision boundary feature extraction)

DBFE is a feature extraction approach for classification based on the decision boundaries [22]. DBFE defines the 'discriminantly informative feature' and 'discriminantly redundant feature' since feature extraction is equivalent to retaining informative features or eliminating redundant features. Lee and Landgrebe [22] revealed that only a portion of the decision boundary is effective for discrimination between different classes. It was also shown that discriminantly informative feature vectors have a component that was normal to the decision boundary at least at one point on the boundary, while discriminantly redundant feature vectors are orthogonal to a vector normal to the decision boundary at every point on the boundary. Both the discriminantly informative and discriminantly redundant features are defined using a decision boundary feature matrix (DBFM), based on which the optimum features can be selected in terms of the accumulation of the eigenvalues.

(3) NWFE (nonparametric weighted feature extraction)

NWFE proposed by Kuo and Landgrebe [23] is based on a nonparametric extension of scatter matrices, and it is an improved version of NDA (nonparametric discriminant analysis) [24]. NWFE focuses on samples near the eventual decision boundary location, and different weights are put on every sample to compute the local means and defining new nonparametric between-class and within-class scatter matrices [23]. The extracted n features are the n eigenvectors with largest n eigenvalues of the following matrix:

$$(S_W^{NW})^{-1} S_B^{NW} \tag{9}$$

where S_W^{NW} and S_B^{NW} are the nonparametric within-class and between-class scatter matrices, respectively.

2.3. LSU (linear spectral unmixing)

LSU is based on the linear mixture model (LMM), which is a widely used method to quantify endmember materials from hyperspectral imagery [25]. The spectrum signature of an observed pixel can be expressed as:

$$z = S\alpha + n \tag{10}$$

where $S = (S_1, S_2, \ldots, S_p)$ is the endmember signature matrix with S_i ($i \in [1, p]$) representing the ith endmember in an image, and $\alpha = (\alpha_1, \alpha_2, \ldots, \alpha_p)^T$ is the abundance vector, where the ith element indicates the proportion of the ith endmember material in the pixel z. The n is noise or measurement error.

There are two constraints due to the physical meaning of LMM: the abundance non-negative and the abundance sum-to-one constraints, which can be expressed as follows,

$$\sum_{i=1}^{p} \alpha_i = 1 \quad \text{and} \quad 0 \le \alpha_i \le 1 \ \text{ for } \ 1 \le i \le p \tag{11}$$

When S is known (supervised linear unmixing), a constrained optimization process can be used to estimate the α by minimizing the estimation error in (10) when the constraints in (11) are satisfied.

In this paper, the abundance components α in the LSU are used to represent the hyperspectral feature space since the number of endmembers is substantially smaller than the number of available bands. Furthermore, the abundance components have clear physical meaning, and hence LSU can be viewed as a feature extraction approach based on the physical constraints. In addition, the abundance components are appropriate to be fed into the object-based classifier since combination of pixel-based and parcel-based physical information results in more meaningful hyperspectral data representation.

3. Object-based subspace classification

3.1. FNEA segmentation

In this study, the fractal net evolution approach [15] is adopted to segment the spectral subspace images extracted from the original hyperspectral data. It utilizes fuzzy set theory to extract the objects of interest, at the scale of interest, segmenting images simultaneously at both fine and coarse scales. FNEA is a bottom-up region merging technique starting from a single pixel. In an iterative way, at each subsequent step, image objects are merged into larger ones. The region merging decision is made with local heterogeneity criterion, which consists of spectral and spatial criteria:

$$h = w \cdot h_{\mathrm{spectral}} + (1 - w) \cdot h_{\mathrm{spatial}} \tag{12}$$

where w is the weight for spectral (against spatial) information with $0 \le w \le 1$, and h_{spectral} and h_{spatial} represent the spectral and spatial change criteria in heterogeneity that occurs when merging two different image objects, respectively. The spectral heterogeneity is defined using the weighted standard deviations:

$$h_{\text{spectral}} = \sum_{b=1}^{B} W_b[N_{\text{Merge}}\sigma_{\text{Merge}} - (N_{\text{Obj1}}\sigma_{\text{Obj1}} + N_{\text{Obj2}}\sigma_{\text{Obj2}})] \quad (13)$$

where B is the dimensionality of subspace, and W_b is the weight of band b. N_{Merge}, N_{Obj1}, and N_{Obj2} represent the numbers of pixels within the merged object, object 1 and object 2, respectively. σ_{Merge}, σ_{Obj1}, and σ_{Obj2} are respective standard deviations. On the other hand, the spatial heterogeneity consists of smoothness and compactness criteria:

$$h_{\text{spatial}} = w_{\text{compact}} \cdot h_{\text{compact}} + (1 - w_{\text{compact}}) \cdot h_{\text{smooth}} \quad (14)$$

with $0 \le w_{\text{compact}} \le 1$ being the weight for the compactness (against smoothness) criterion. The spatial heterogeneity is also calculated by comparing the difference between the situation after and before the merge, and the compactness and smoothness are defined as,

$$h_{\text{smooth}} = N_{\text{Merge}} \cdot \frac{l_{\text{Merge}}}{r_{\text{Merge}}} - \left(N_{\text{Ob1}} \cdot \frac{l_{\text{Ob1}}}{r_{\text{Ob1}}} + N_{\text{Ob2}} \cdot \frac{l_{\text{Ob2}}}{r_{\text{Ob2}}}\right) \quad (15)$$

$$h_{\text{compact}} = N_{\text{Merge}} \cdot \frac{l_{\text{Merge}}}{\sqrt{N_{\text{Merge}}}} - \left(N_{\text{Ob1}} \cdot \frac{l_{\text{Ob1}}}{\sqrt{N_{\text{Ob1}}}} + N_{\text{Ob2}} \cdot \frac{l_{\text{Ob2}}}{\sqrt{N_{\text{Ob2}}}}\right) \quad (16)$$

where l is the object perimeter and r is the perimeter of the rectangles that contain the object. When a possible merge of a pair of image objects is examined, the fusion heterogeneity value h between those two objects is calculated and compared to the scale parameter T. The two objects are merged when $H < T$. The scale parameter is a measure of the maximum change in heterogeneity that may occur when merging two image objects.

3.2. Object-based subspace classification using SVM

The basic idea of OBA (object-based analysis) is to group the spatially adjacent pixels into spectrally homogeneous objects and then conduct classification on objects (not pixels) as the minimum processing unit. OBA is potential to reduce the local spectral variation in homogeneous regions, avoid the salt–pepper effect of pixel-based methods, and mimic human perception in identifying objects. Most of existing literature about the OBA technique was related to the high spatial-resolution multispectral image [26–28], since it is able to exploit rich spatial information contained in images. It should be noted that high spatial-resolution images often include several spectral bands. For instance, the well-known high spatial-resolution satellite sensors such as Quickbird, IKONOS, and GeoEye only contain four spectral bands. However, hyperspectral data always includes hundreds of channels, therefore, the OBA approach cannot be directly applied to hyperspectral data since the hyper-dimensional spectral space will significantly increase the computational time of object-based analysis. In this context, this study proposed to integrate the subspace analysis and the object-based classification technique in order to exploit both spectral and spatial information contained in the hyperspectral data and reduce computational cost of OBA.

The proposed object-oriented subspace analysis with SVM classifiers is described as follows:

Step 1, Preprocessing: subspace feature extraction from the original hyperspectral channels. This step aims to extract hyperspectral information and reduce computational cost for subsequent processing.

Step 2, FNEA segmentation: object extraction from the subspace images. FNEA algorithm is used to yield meaningful objects or segments by considering both spectral and spatial criteria.

Step 3, Spectral characteristics of objects: after *Step* 2, the subspace image has been represented based on objects rather than pixels. Accordingly, the pixel-by-pixel spectral information within each segment is integrated for object-based features. In this paper, the spectral characteristic for each segment is calculated by averaging the spectral vectors of all pixels within this segment:

$$F_b(i) = \frac{1}{n}\sum_{x \in i} F_b(x) \quad \text{with} \quad F(x) = \{F_1(x), \ldots, F_b(x), \ldots, F_B(x)\} \quad (17)$$

where $F(x)$ is the spectral vector with B-dimensional subspace for pixel x. After this step, each segment i is represented using an averaged spectral vector with dimension of B.

Step 4, SVM-based classification: this step aims to classify each segment using SVM classifier. The RBF (radial basis function) kernel is chosen due to its effectiveness in many classification problems. The regularization parameter and the spread factor of RBF kernel are determined using cross-validation approach.

Step 5, Accuracy assessment.

4. Experiments and analysis

4.1. Experiments on the AVIRIS dataset

This experiment was conducted on the AVIRIS hyperspectral data set over Indian Pines. From the 220 spectral channels acquired by the AVIRIS sensor, 11 bands were discarded because they were affected by atmospheric problems. The image shows a typical agricultural site with many kinds of crops. The RGB image and the ground-truth reference were displayed in Fig. 2. The numbers of training-test samples were listed in Table 1.

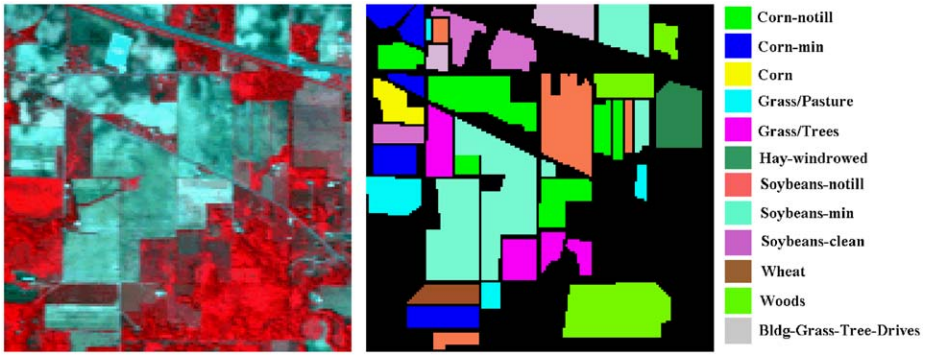

Fig. 2. RGB composites of the Indian Pines (channels 47, 24, and 14 for RGB), and the ground-truth reference map.

Table 1
Number of training and test samples for the AVIRIS data set.

Class	Label	No. of training samples	No. of test samples
Corn-notill	C1	143	1434
Corn-min	C2	83	834
Corn	C3	23	234
Grass/pasture	C4	50	497
Grass/trees	C5	75	747
Hay-windrowed	C6	49	489
Soybeans-notill	C7	97	968
Soybeans-min	C8	247	2468
Soybeans-clean	C9	61	614
Wheat	C10	21	212
Woods	C11	129	1294
Bldg-grass-tree-drives	C12	38	380
Total	–	1016	10,171

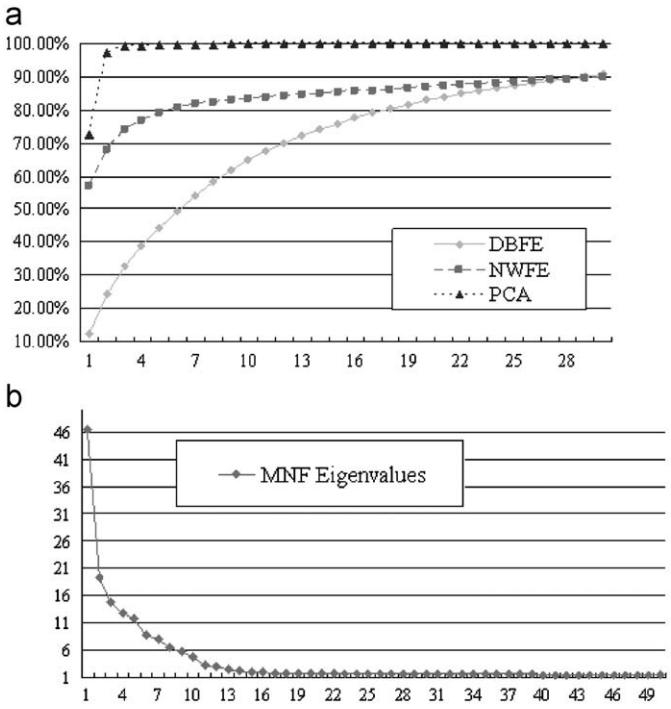

Fig. 3. (a) The cumulative eigenvalues in percentage for the DBFE, NWFE and PCA transformations, and (b) MNF eigenvalues for the AVIRIS data set.

4.1.1. Subspace feature extraction

The cumulative eigenvalues in percentage for the PCA, DBFE and NWFE were shown in Fig. 3(a), where the x and y axes represented the dimensionality of subspace and the cumulative percentages, respectively. From the figure, it can be seen that only 3-dimensional PCA subspace contains over 99% variance of the original hyperspectral data, while 15-dimensional NWFE and DBFE features give 85% and 75% variance, respectively. The eigenvalues of MNF transformation were arranged in Fig. 3(b), from which we can choose the first 15-dimensional MNF features corresponding to the largest 15 eigenvalues as the spectral subspace. The MNF eigenimages with near-unity eigenvalues can be viewed as noise-dominated features and hence removed. Table 2 shows the eigenvalues of DAFE transformation. It should be noted that at maximum 11-dimensional subspace is available for DAFE since the maximum rank of Σ_B is $(N-1)$ for an N-class problem. In addition, 12-dimensional abundance components were obtained based on the constrained LSU method, and it must be kept in mind that the dimensionality of the LSU-based subspace is equivalent to the number of information classes.

Table 2
Eigenvalues of the DAFE transformation.

Component	Eigenvalue	Cumulative percentage (%)
1	18.2056	44.58
2	9.8312	68.66
3	5.1552	81.28
4	2.5056	87.42
5	1.5092	91.11
6	1.2620	94.20
7	0.9666	96.57
8	0.7833	98.49
9	0.3354	99.31
10	0.1912	99.78
11	0.0908	100.0

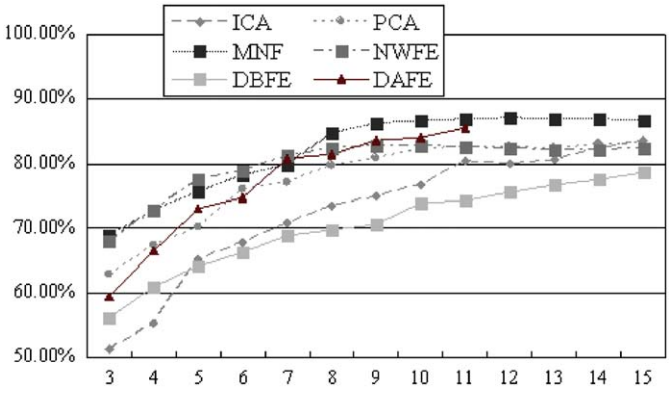

Fig. 4. Overall accuracies in percentage for the pixel-based subspace classification using different feature images.

4.1.2. Comparison of pixel-based and object-based subspace classification

The pixel-based classification accuracies were shown in Fig. 4. The overall accuracies (OA) based on the confusion matrix were used to assess the classification results. The statistics in Fig. 4 were obtained using a pixel-by-pixel SVM classification without considering the spatial relationship of neighboring pixels. In the figure, the x and y axes represented the dimensionality of subspace and the OA, respectively. The first comment to this figure is that MNF and DAFE outperformed other FE methods, since they gave higher accuracies with less dimensionality. It can be found that the supervised methods (e.g. DBFE, NWFE) did not necessarily outperform the unsupervised methods (e.g. PCA, ICA and MNF), which may be due to the subsequent use of a supervised classifier (SVM). It can be also observed that overall accuracies did not improve much after 10-dimensional subspace was included in the feature sets for MNF, PCA and NWFE. Considering that the pixel-wise classification of SVM with the originally 209-dimensional AVIRIS channels gave OA=77.7%, it can be said that subspace analysis is effective in extracting spectral information from the hyperspectral data, furthermore, it is able to reduce the computational cost for the subsequent OBA classification.

The pixel-based (P) and object-based (O) classification results were compared in Table 3, where the overall accuracies (OA) for different FE algorithms were reported. The table shows that the object-oriented subspace classification can provide substantially

Table 3
Comparison between pixel-based and object-based subspace classification ('O' and 'P' denote object-based and pixel-based classification).

Dimension of subspace	ICA		PCA		MNF		NWFE		DBFE		DAFE	
	P	O	P	O	P	O	P	O	P	O	P	O
3	51.3	69.5	63.0	67.8	69.0	74.8	68.1	74.0	56.3	69.5	59.5	79.8
4	55.4	74.4	67.4	73.9	72.9	77.6	72.8	81.3	61.1	75.9	66.6	89.0
5	65.3	80.5	70.3	81.0	75.5	81.4	77.6	85.6	64.1	77.0	73.0	92.1
6	67.9	82.8	76.0	85.4	78.1	87.8	78.9	86.8	66.4	79.7	74.9	92.8
7	70.8	86.7	77.1	87.1	79.8	89.5	81.3	88.2	69.0	82.2	80.9	96.7
8	73.5	87.9	79.7	90.9	84.7	93.3	82.4	89.8	69.8	84.2	81.5	97.5
9	74.9	89.0	80.9	91.7	86.3	94.0	82.7	92.2	70.8	84.7	83.7	97.7
10	76.7	91.0	82.4	94.4	86.6	94.8	82.8	92.9	73.8	87.5	84.1	97.6

higher accuracies than the pixel-wise classification, regardless of the dimensionality of subspace images. With the OBA classification, the OA improvements were 14.2%, 12.0%, 8.3%, 10.2%, 13.7%, and 13.5% for 10-dimensional ICA, PCA, MNF, NWFE, DBFE and DAFE features, respectively. The OBA-based DAFE achieved over 97% overall accuracy with less than 10-dimensional subspace, in addition, the OBA-based PCA and MNF features gave over 92% overall accuracies. Therefore, it can be stated that the object-based analysis can exploit the spatial relationship of pixels effectively and give much more accurate classification results.

Fig. 5 compared the classification maps of the PCA, MNF, NWFE, LSU, DBFE and DAFE features for the pixel-based and object-based classification. From the figure, it can be observed that the OBA method reduced the pepper–salt effects resulted from the pixel-wise classification, and it avoided the misclassifications and uncertainty in homogeneous regions. In addition, the OBA method classified the image based on objects, consequently, it is more appropriate for the vector-based post-processing and GIS (Geographic Information System) spatial analysis. Table 4 provided the class-specific accuracies for different subspace features with and without OBA, and the accuracies obtained by all-bands AVIRIS hyperspectral data (209 channels) were used for comparison.

4.1.3. Comparison with the texture-based classification

Textural measures are compared because they have been proven an effective approach for spatial information extraction. Therefore, in order to further validate the proposed OBA subspace classification method, some texture features (e.g. GLCM and wavelet features) were implemented as benchmarks. Three subspace images: PCA (10-dimensional), MNF (10-dimensional) and DAFE (11-dimensional) features, were selected for the texture analysis considering their good performance in both pixel-based and object-based classification. As suggested in [29], four GLCM measures, homogeneity, angular second moment, dissimilarity and entropy, were used to extract texture features from each band of the PCA, MNF and DAFE subspace:

$$\text{Homogeneity}: \text{HOM} = \sum_i \sum_j \frac{P(i,j)}{1+(i-j)^2} \tag{18}$$

$$\text{Angular second moment}: \text{ASM} = \sum_i \sum_j (P(i,j))^2 \tag{19}$$

$$\text{Entropy}: \text{ENT} = -\sum_i \sum_j P(i,j)\log(P(i,j)) \tag{20}$$

$$\text{Dissimilarity}: \text{DIS} = -\sum_i \sum_j P(i,j)|i-j| \tag{21}$$

where (i,j) is the coordinate in the co-occurrence matrix space and $P(i,j)$ is the co-occurrence matrix value at (i,j). The texture features were stacked with the spectral subspace images, leading to 50-, 50-, and 55-dimensional spectral-textural hybrid feature space for PCA, MNF and DAFE, respectively. The resulted hybrid features were classified using SVM classifiers.

On the other hand, the stationary wavelet transformation was also used to extract the multiscale texture features from different subspace images. The following equation is defined to extract the multilevel wavelet-based features:

$$F = \left\{ F_l(b) = \frac{H_l(b)+V_l(b)+D_l(b)}{3}, \quad l=[1,L], \ \ b=[1,B] \right\} \tag{22}$$

where l and b represent the level of wavelet decomposition and the bth band of subspace, respectively. $H_l(b)$, $V_l(b)$, and $D_l(b)$ indicate the horizontal, vertical and diagonal wavelet coefficients for level l and band b. The wavelet coefficients in different directions were summed to represent texture information and spectral variation [30,31]. The multilevel wavelet textures were combined with the spectral subspace images and the resulted hybrid vectors were then classified using SVMs. In this experiment, three levels of wavelet decomposition were used (L=3).

Their overall accuracies were compared in Fig. 6. It was seen that both wavelet and GLCM textural features improved the pixel-wise classification. The accuracy improvements resulted from the wavelet textures were 2.6%, 1.9%, and 0.3% for PCA, MNF and DAFE, respectively, and the respective improvements from the GLCM textures were 9.2%, 6.0%, and 7.7%. However, it can be clearly seen that the object-based classification give the most accurate results. Especially, it should be noted that the dimensionality of the object-based features is equivalent to that of the subspace (10, 10 and 11 for PCA, MNF and DAFE), however, the utility of GLCM and wavelet textures substantially increased the dimensionality of subspace (50, 50 and 55 for PCA, MNF and DAFE). Therefore, it can be said that the proposed OBA subspace classification algorithm is more effective in simultaneously exploit spectral and spatial information in terms of accuracies and computational cost.

4.2. Experiments on the ROSIS dataset

In order to further evaluate the proposed algorithm, another airborne hyperspectral dataset was used. The dataset used in this experiment was collected in the framework of the HySens project, managed by DLR (the German Aerospace Center) and sponsored by the European Union. The images were acquired by the ROSIS sensor during a flight campaign over Pavia, northern Italy (45°11′N, 9°9′E), on the 8th of July 2002. The ROSIS dataset recorded the 0.43–0.86 μm region of the visible and infrared

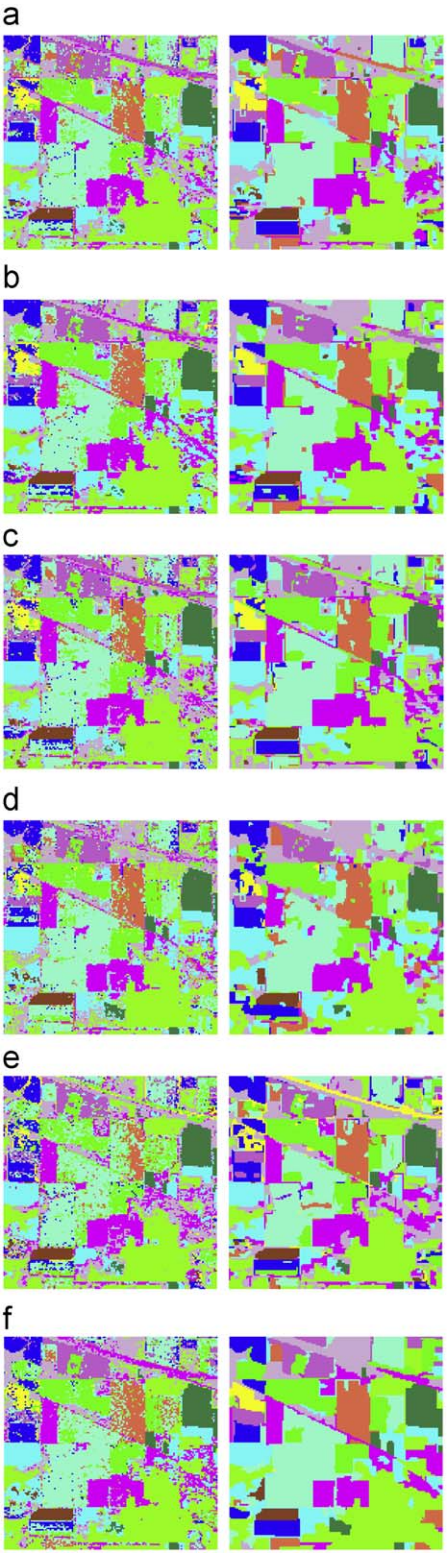

Fig. 5. Classification maps for (a) PCA, (b) MNF, (c) NWFE, (d) LSU, (e) DBFE, and (f) DAFE features for the pixel-based (left) and object-based (right) classification.

Table 4
Class-specific accuracies for different subspace features.

Class no.	209 Bands	PCA		MNF		NWFE		LSU		DAFE	
		P	O	P	O	P	O	P	O	P	O
C1	69.9	77.9	90.6	86.6	92.8	79.0	92.3	82.1	86.6	84.8	97.2
C2	53.7	61.0	92.1	70.4	96.4	64.8	91.5	50.8	89.1	73.3	96.8
C3	66.2	67.5	92.3	71.8	85.0	72.7	92.7	43.2	55.1	71.4	94.4
C4	87.1	93.4	93.8	94.6	94.4	93.2	95.8	89.7	88.7	93.2	99.2
C5	92.6	96.0	99.3	99.2	100.0	97.7	98.5	96.7	96.0	97.7	99.1
C6	99.4	99.4	99.4	99.6	99.2	99.6	99.6	99.2	98.0	99.4	100.0
C7	61.7	63.1	88.2	70.7	87.9	62.9	72.3	65.9	80.7	68.3	91.9
C8	84.1	85.7	97.1	85.9	94.7	83.5	95.8	86.4	91.5	85.1	98.7
C9	60.4	82.3	88.6	88.3	95.6	84.5	94.5	88.3	89.9	83.4	96.4
C10	90.1	98.1	99.5	99.1	98.1	99.1	99.5	98.6	94.8	99.5	99.1
C11	96.1	97.6	98.5	97.4	98.1	96.1	96.3	92.8	98.1	94.4	99.7
C12	55.0	60.5	91.1	76.8	93.4	66.3	92.1	75.0	94.5	83.4	99.7
OA	77.7	82.4	94.4	86.6	94.8	82.8	92.9	82.2	90.2	85.5	97.7

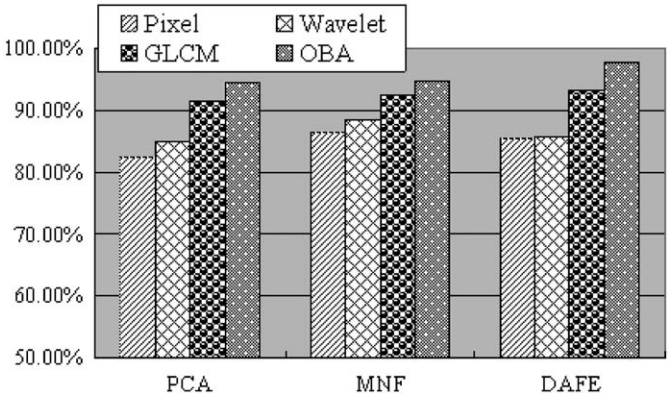

Fig. 6. Overall accuracies of the pixel-based, texture-based and object-based classification for PCA (10-dimensional), MNF (10-dimensional) and DAFE (11-dimensional) subspace components.

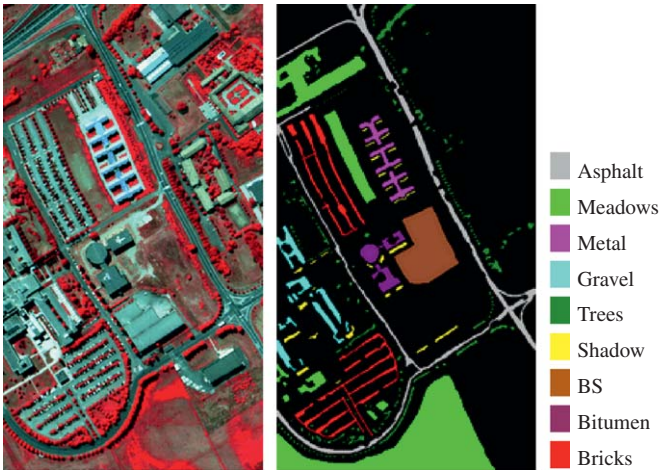

Fig. 7. RGB composites of the Pavia University (channels 90, 60, and 40 for RGB), and the ground-truth reference.

spectrum with spatial resolution of 1.3 m. The test image in this experiment is around the Engineering School at the University of Pavia with 103 hyperspectral channels. The test image and the ground-truth reference map were shown in Fig. 7, and the numbers of training-test samples were listed in Table 5.

Five subspace feature extraction methods were utilized in this experiment: (1) unsupervised FE: PCA, ICA, (2) supervised FE: NWFE, and (3) the LSU model. The accumulative eigenvalues in percentage for PCA and NWFE were shown in Fig. 8(a), and the eigenvalues of MNF transformation were shown in Fig. 8(b).

Table 5
The training and test samples for Pavia University data.

Classes	No. of training set	No. of test set
Trees	524	3064
Asphalt	548	6631
Bitumen	375	1330
Gravel	392	2099
Metal sheets	265	1345
Shadow	231	947
Bricks	514	3682
Meadows	540	18,649
BS (bare soil)	532	5029
Total	3921	42,776

Table 6
Overall accuracies in percentage for pixel-based, OBA-based, and GLCM-based classification of Pavia University dataset.

Subspace	All	PCA	ICA	MNF	NWFE	LSU
No. of dimension	103	4	9	9	9	9
Pixel-based	73.5	68.0	76.3	71.5	75.0	63.5
No. of dimensions	NA	20	45	45	45	45
GLCM-based	NA	80.0	76.9	77.7	80.2	50.3
No. of dimensions	NA	4	9	9	9	9
OBA-based	NA	82.2	85.5	84.5	85.8	73.6

"All" indicates the original 103-dimensional hyperspectral channels.

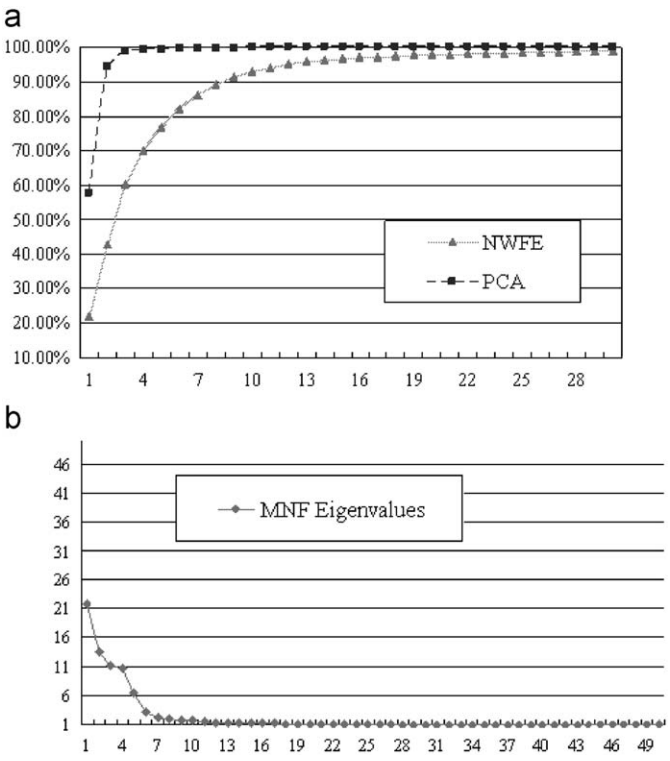

Fig. 8. (a) The cumulative eigenvalues in percentage for PCA and NWFE, and (b) MNF eigenvalues for the Pavia University data set.

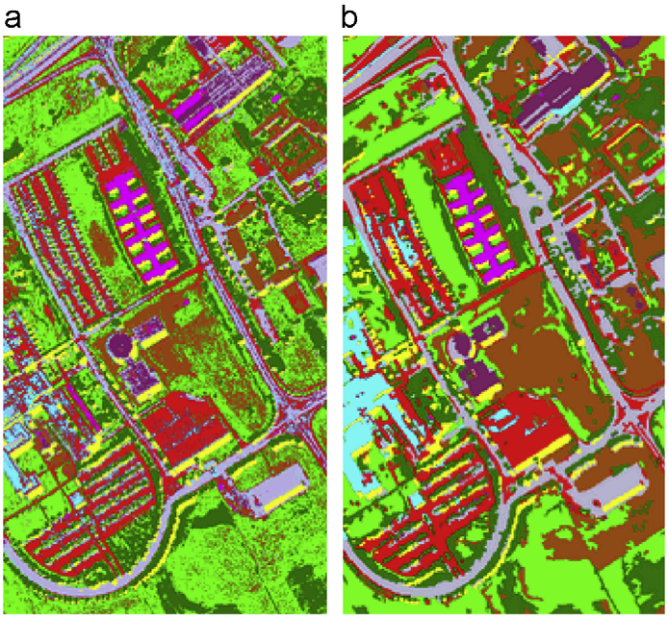

Fig. 9. (a) and (b) are pixel-based and object-based classification maps for NWFE subspace features, respectively.

According to the statistics in Fig. 8, we can determine the appropriate subspace dimensionality. In this experiment, 4-dimensional PCA and 9-dimensional NWFE images were used since they contained over 99% and 90% accumulative eigenvalues, respectively. 9-dimensional MNF images were used since the remaining eigenvalues were near unity and hence resulted in noise-dominated images. In addition, the dimensions of independent components (ICs) and abundance components were equivalent to the number of information classes (in this experiment, the number is 9).

The pixel-based, OBA-based, and GLCM texture-based classifications were compared in Table 6, where both accuracies (%) and dimensionality of features were shown. From the statistics in the table, we can obtain the following observations:

(1) By observing the results of pixel-based classification, it can be found that the ICA and NWFE subspace features gave higher accuracies than the original hyperspectral data with 103 channels. The improvements of OA were 2.8% and 1.5%, respectively. In addition, the MNF subspace features achieved comparable results with the original hyperspectral data.

(2) When the GLCM textures were combined with the subspace spectral features, overall accuracies increased except the LSU, the additional accuracies achieved by GLCM were 12.0%, 0.6%, 6.2%, and 5.2% for PCA, ICA, MNF and NWFE, respectively. It was shown that GLCM textures were able to exploit the spatial relationship of neighboring pixels and gave more accurate results than the spectral classification alone.

(3) From the results of OBA-based classification, it was clearly seen that the object-oriented analysis could be successfully applied to subspace image classification, and give substantially higher accuracies. Compared with the pixel-based classification, the improvements of OA achieved by the OBA algorithm were 14.2%, 9.2%, 13.0%, 10.8%, and 10.1% for PCA, ICA, MNF, NWFE and LSU, respectively. It was also noted that the OBA approach obtained higher accuracies than GLCM but with much smaller feature dimensionality. The ICA-, MNF- and NWFE-based OBA classification gave about 85% overall accuracy, which were very promising considering that the OA

of original 103-dimensional data was 73.5%. The classification maps before and after the OBA for NWFE subspace were compared in Fig. 9.

5. Conclusion

The contribution of this paper is to investigate the object-oriented analysis for hyperspectral image classification, in order to simultaneously exploit the spectral and spatial information contained in the images. To this end, the subspace analysis techniques are used to reduce the computational cost, since the object-based classification is time-consuming and unacceptable for hyperspectral data with hundreds of channels. On the other hand, subspace analysis is able to reduce the information redundancy in hyperspectral data as the huge spectral channels are highly correlated. Therefore, we proposed to integrate the subspace analysis and object-oriented classification for hyperspectral image interpretation.

Two hyperspectral datasets were used for validation of the proposed method. The first experiment was conducted on the AVIRIS airborne hyperspectral data set over the Indian Pines with 209 channels and spatial resolution of 20 m (agricultural area at the west of West Lafayette). The other dataset is the Pavia University image acquired by the ROSIS airborne sensor with 103 channels and spatial resolution of 1.3 m (urban region at Pavia city, northern of Italy). The experimental results revealed that:

(1) The subspace images were effective in extracting spectral information from the hyperspectral data. This conclusion was supported since PCA, MNF, NWFE, DAFE, LSU features gave higher accuracies than the 209-dimensional AVIRIS image, and ICA, MNF and NWFE images achieved comparable or higher accuracies than the 103-dimensional ROSIS data, but with much smaller dimensionality.
(2) The OBA-based subspace features gave much more accurate mapping results than the pixel-based subspace in both agricultural and urban regions. It can be said that the integration of subspace analysis and object-based processing is effective for spectral/spatial information extraction and classification from hyperspectral data. In addition, in comparison with results obtained by GLCM textures, the proposed approach gave obviously higher accuracies but with much smaller feature dimensionality.

Acknowledgment

This work is supported by the Natural Science Foundation of China under Grants 40771139 and 40930532.

References

[1] M.A. Karaska, R.L. Hugenin, J.L. Beacham, M. Wang, J.R. Jenson, R.S. Kaufmann, AVIRIS measurements of chlorophyll, suspended minerals, dissolved organic carbon, and turbidity in the Neuse River, North Carolina, Photogrammetric Engineering and Remote Sensing 70 (1) (2004) 125–133.
[2] A. Srivastava, X. Liu, Tools for application-driven linear dimension reduction, Neurocomputing 67 (2005) 136–160.
[3] R. Saegusa, H. Sakano, S. Hashimoto, Nonlinear principal component analysis to preserve the order of principal components, Neurocomputing 61 (2004) 57–70.
[4] W. Zuo, K. Wang, D. Zhang, H. Zhang, Combination of two novel LDA-based methods for face recognition, Neurocomputing 70 (2007) 735–742.
[5] A. Mohan, G. Sapiro, E. Bosch, Spatially coherent nonlinear dimensionality reduction and segmentation of hyperspectral images, IEEE Geoscience and Remote Sensing Letters 4 (2) (2007) 206–210.
[6] Q. Du, C. Chang, A linear constrained distance-based discriminant analysis for hyperspectral image classification, Pattern Recognition 34 (2) (2001) 361–373.
[7] X. Huang, L. Zhang, An adaptive mean-shift analysis approach for object extraction and classification from urban hyperspectral imagery, IEEE Transactions on Geoscience and Remote Sensing 46 (12) (2008) 4173–4185.
[8] Y. Liu, Wavelet feature extraction for high-dimensional microarray data, Neurocomputing 72 (2009) 985–990.
[9] C. Zheng, D. Huang, L. Shang, Feature selection in independent component subspace for microarray data classification, Neurocomputing 69 (2006) 2407–2410.
[10] D. Tao, X. Li, X. Wu, S. Mayband, Tensor rank one discriminant analysis—a convergent method for discriminant miltilinear subspace selection, Neurocomputing 71 (2008) 1866–1882.
[11] D. Tao, X. Li, X. Wu, S.J. Maybank, Geometric mean for subspace selection, IEEE Transactions on Pattern Analysis and Machine Intelligence 31 (2) (2009) 260–274.
[12] X. Li, S. Lin, S. Yan, D. Xu, Discriminant locally linear embedding with high-order tensor data, IEEE Transactions on Systems, Man, and Cybernetics, Part B, Cybernetics 38 (2) (2008) 342–352.
[13] X. Huang, L. Zhang, A comparative study of spatial approaches for urban mapping using hyperspectral ROSIS images over Pavia city, northern of Italy, International Journal of Remote Sensing 30 (12) (2009) 3205–3221.
[14] J.M. Duarte-Carvajalino, G. Sapiro, M. Velez-Reyes, P.E. Castillo, Multiscale representation and segmentation of hyperspectral imagery using geometric partial differential equations and algebraic multigrid methods, IEEE Transactions on Geoscience and Remote Sensing 46 (8) (2008) 2418–2434.
[15] G.J. Hay, T. Blaschke, D.J. Marceau, A. Bouchard, A comparison of three image-object methods for the multiscale analysis of landscape structure, ISPRS Journal of Photogrammetry and Remote Sensing 57 (5) (2003) 327–345.
[16] C. Cortes, V. Vapnik, Support vector networks, Machine Learning 20 (3) (1995) 273–297.
[17] X. Huang, L. Zhang, P. Li, Classification and extraction of spatial features in urban areas using high resolution multispectral imagery, IEEE Geoscience and Remote Sensing Letters 4 (2) (2007) 260–264.
[18] J.M.P. Nascimento, J.M.B. Dias, Dose independent component analysis play a role in unmixing hyperspectral data?, IEEE Transactions on Geoscience and Remote Sensing 43 (1) (2005) 175–187.
[19] A.J. Bell, T.J. Sejnowski, An information maximization approach to blind deconvolution, Neural Computation 10 (1995) 215–234.
[20] A.A. Green, M. Berman, P. Switzer, M.D. Craig, A transformation for ordering multispectral data in terms of image quality with implications for noise removal, IEEE Transactions on Geoscience and Remote Sensing 26 (1) (1988) 65–74.
[21] D.A. Landgrebe, Signal Theory Methods in Multispectral Remote Sensing, Wiley, Hoboken, NJ, 2003.
[22] C. Lee, D.A. Landgrebe, Feature extraction based on decision boundaries, IEEE Transactions on Pattern Analysis and Machine Intelligence 15 (4) (1993) 388–400.
[23] B. Kuo, D.A. Landgrebe, Nonparametric weighted feature extraction for classification, IEEE Transactions on Geoscience and Remote Sensing 42 (5) (2004) 1096–1105.
[24] K. Fukunaga, M. Mantock, Nonparametric discriminant analysis, IEEE Transactions on Pattern Analysis and Machine Intelligence PAMI-5 (1983) 671–678.
[25] Q. Du, N. Raksuntorn, S.S. Cai, R.J. Moorhead, Color display for hyperspectral imagery, IEEE Transactions on Geoscience and Remote Sensing 46 (6) (2008) 1858–1866.
[26] A.K. Shackelford, C.H. Davis, A combined fuzzy pixel-based and object-based approach for classification of high-resolution multispectral data over urban areas, IEEE Transactions on Geoscience and Remote Sensing 41 (10) (2003) 2354–2363.
[27] Y. Tarabalka, J.A. Benediktsson, J. Chanussot, Spectral-spatial classification of hyperspectral imagery based on partitional clustering techniques, IEEE Transactions on Geoscience and Remote Sensing 47 (8) (2009) 2973–2987.
[28] D. Stow, A. Lopez, C. Lippitt, S. Hinton, J. Weeks, Object-based classification of residential land use within Accra, Ghana based on QuickBird satellite data, International Journal of Remote Sensing 28 (22) (2007) 5167–5173.
[29] X. Huang, L. Zhang, P. Li, An adaptive multiscale information fusion approach for feature extraction and classification of IKONOS multispectral imagery over urban areas, IEEE Geoscience and Remote Sensing Letters 4 (4) (2007) 654–658.
[30] Y.O. Ouma, T.G. Ngigi, R. Tateishi, On the optimization and selection of wavelet texture for feature extraction from high-resolution satellite imagery with application towards urban-tree delineation, International Journal of Remote Sensing 27 (1) (2006) 73–104.
[31] X. Huang, L. Zhang, P. Li, A multiscale feature fusion approach for classification of very high resolution satellite imagery, International Journal of Remote Sensing 29 (20) (2008) 5923–5941.

Liangpei Zhang received the B.S. degree in physics from Hunan Normal University, ChangSha, China, in 1982, the M.S. degree in optics from the Xi'an Institute of Optics and Precision Mechanics of Chinese Academy of Sciences, Xi'an, China, in 1988, and the Ph.D. degree in Photogrammetry and Remote Sensing from Wuhan University, Wuhan, China, in 1998.

From 1997 to 2000, he was a professor of School of the Land Sciences in Wuhan University, Wuhan. In August 2000, he joined the State Key Laboratory of Information Engineering in Surveying, Mapping and Remote Sensing, Wuhan University, Wuhan, as a professor and head of the Remote Sensing Section. Since 2007, he has been nominated as a 'ChangJiang Scholar' professor (Chair Professor) by the Education Ministry of China. He has published more than 150 research papers. His research interests include hyperspectral remote sensing, high resolution remote sensing, image processing, and artificial intelligence.

Dr. Zhang has served as Co-Chair of the SPIE Series Conferences on Multispectral Image Processing and Pattern Recognition (MIPPR), the Conference on Asia Remote Sensing in 1999, editor of the MIPPR01, MIPPR05, Geoinformatics Symposiums, associate editor of Geo-spatial Information Science Journal, Chinese National Committee for the International Geosphere–Biosphere Programme, and Executive Member for China Society of Image and Graphics.

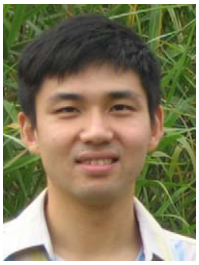

Xin Huang received the Ph.D. degree in the State Key Laboratory of Information Engineering in Surveying, Mapping and Remote Sensing (LIESMARS), Wuhan University, in 2009.

He is currently an assistant professor in the LIESMARS, Wuhan University. He has been the first author of over 10 scientific publications in referred international journals. His research interests include hyperspectral data analysis, high resolution image processing, pattern recognition and remote sensing applications.

Dr. Huang was a referee of IEEE International Geoscience & Remote Sensing Symposium, International Journal of Remote Sensing, and Photogrammetric Engineering and Remote Sensing.